

See discussions, stats, and author profiles for this publication at: <https://www.researchgate.net/publication/14457965>

Structural coupling of inhibitory regions flanking the ETS domain of murine Ets-1

ARTICLE *in* PROTEIN SCIENCE · FEBRUARY 2008

Impact Factor: 2.85 · DOI: 10.1002/pro.5560050214 · Source: PubMed

CITATIONS

39

READS

8

5 AUTHORS, INCLUDING:



[Logan W Donaldson](#)

York University

29 PUBLICATIONS 1,374 CITATIONS

[SEE PROFILE](#)



[Barbara J Graves](#)

University of Utah

70 PUBLICATIONS 6,187 CITATIONS

[SEE PROFILE](#)

Structural coupling of the inhibitory regions flanking the ETS domain of murine Ets-1

JACK J. SKALICKY,^{1,3} LOGAN W. DONALDSON,¹ JEANNINE M. PETERSEN,²
BARBARA J. GRAVES,² AND LAWRENCE P. McINTOSH¹

¹ The Department of Biochemistry and Molecular Biology and the Department of Chemistry,
University of British Columbia, Vancouver, British Columbia V6T 1Z3, Canada

² The Department of Oncological Sciences, Division of Molecular Biology and Genetics,
University of Utah School of Medicine, Salt Lake City, Utah 84132

(RECEIVED October 9, 1995; ACCEPTED November 11, 1995)

Abstract

Several members of the *ets* gene family of transcription factors show negative regulation of DNA binding by intramolecular interactions. A structural mechanism for this auto-inhibition is investigated using a 161-residue N-terminal deletion mutant of murine Ets-1, Ets-1ΔN280. This protein shows a similar reduced affinity for DNA as native Ets-1 because it contains the ETS domain in context of the flanking amino- and carboxy-terminal regions that together mediate repression of DNA binding. The secondary structure of Ets-1ΔN280 was determined using NMR chemical shift, NOE, J coupling, and amide hydrogen exchange information. In addition to the winged helix-turn-helix ETS domain, Ets-1ΔN280 contains two α -helices in the amino-terminal inhibitory region and one α -helix in the carboxy-terminal inhibitory region. Chemical shift comparisons were made between this protein and an activated form of Ets-1 lacking the amino-terminal inhibitory region. The spectral differences demonstrate that the amino- and carboxy-terminal inhibitory sequences are structurally coupled to one another, thus explaining the observation that both regions are required for the repression of DNA binding. Furthermore, these data show that the inhibitory sequences also interact directly with the first helix of the intervening ETS domain, thereby providing a pathway for the repression of DNA binding. These results lead to a model of an inhibitory module in Ets-1 composed of both the amino- and carboxy-terminal regions interfaced with the ETS domain. This establishes the structural framework for understanding the intramolecular inhibition of Ets-1 DNA binding.

Keywords: allosteric; DNA binding; ETS domain; Ets-1 and Ets-2; intramolecular inhibition; NMR; protein structure; winged helix-turn-helix

DNA binding, activation, and oligomerization associated with a particular transcription factor may be governed by its subcellular localization, posttranslational modifications, ligand binding, and protein-protein interactions. Recently, data have

Reprint requests to: Lawrence McIntosh, Department of Biochemistry, 2146 Health Sciences Mall, University of British Columbia, Vancouver, British Columbia V6T 1Z3, Canada; e-mail: mcintosh@otter.biochem.ubc.ca.

³ Present address: Department of Chemistry, SUNY-Buffalo, Buffalo, New York 14260-3000.

Abbreviations: ets, E26 transformation specific; Ets-1ΔC428, the carboxy-terminal deletion fragment of murine Ets-1 consisting of residues 1–428; Ets-1ΔN280, the amino-terminal deletion fragment of murine Ets-1 consisting of residues 280–440; Ets-1ΔN331, the amino-terminal deletion fragment of murine Ets-1 consisting of residues 331–440; FID, free induction decay; HSQC, heteronuclear single quantum correlation; NOESY, nuclear Overhauser effect spectroscopy; TOCSY, total correlation spectroscopy; IPTG, isopropyl- β -D-thiogalactopyranoside; DTT, dithiothreitol; pH*, the observed pH meter reading without correction for isotope effects; wHTH, winged helix-turn-helix; HSF, heat shock transcription factors; DSS, 2,2-dimethyl-2-silapentane-5-sulfonate, sodium salt.

emerged demonstrating that transcription factors can also negatively autoregulate their own activity. This phenomenon of intramolecular inhibition is supported by a growing body of evidence suggesting that the functional characteristics of an isolated transcription factor domain can be different when compared with those of the intact protein. For example, deletions or mutations outside the DNA-binding domains of p53, NF κ B, and TATA-Binding Protein (TBP) substantially alter the affinity of these regulatory proteins for DNA (Lieberman et al., 1991; Hupp et al., 1992; Grimm & Baeuerle, 1993). In addition, trimerization of human and *Drosophila* heat shock transcription factors, HSF, is suppressed by intramolecular coiled-coil interactions (Rabindran et al., 1993). Repression of the activation domain of the transcription factor CRP2 (C/EBP β) has also been shown to be modulated by adjacent sequences (Kowenz-Leutz et al., 1994; Williams et al., 1995). These observations challenge the view of transcription factors as composite proteins comprised of autonomous functional domains. Furthermore, it stresses the importance of characterizing the domains from these proteins both in isolation and in their native structural context.

to understand fully the roles that they play in the regulation of gene expression.

The *ets* family of transcriptional regulators has emerged as a model system for the auto-inhibition of DNA recognition. Members of this family are characterized by a highly conserved 85-amino acid DNA-binding region termed the ETS domain (Karim et al., 1990; Macleod et al., 1992; Janknecht & Nordheim, 1993; Waslyk et al., 1993). Recent NMR studies have shown that the ETS domain is a winged helix-turn-helix DNA-binding motif (Donaldson et al., 1994, 1996; Liang et al., 1994a, 1994b). In several members of the *ets* family, the intrinsic DNA-binding activity of the ETS domain is repressed by sequences that lie outside this domain. Specifically, deletion and partial proteolysis experiments demonstrate that the truncated *ets* proteins Sap-1, Elk-1, Erp, Net, Ets-1, and Ets-2 all have higher binding activity than the full-length native proteins (Dalton & Treisman, 1992; Hagman & Grosschedl, 1992; Lim et al., 1992; Nye et al., 1992; Waslyk et al., 1992; Giovane et al., 1994; Janknecht et al., 1994; Lopez et al., 1994).

Ets-1, the founding member of the *ets* family, has been shown to contain inhibitory sequences amino- and carboxy-terminal to the ETS domain. Deletion of either region results in as much as a 10–20-fold increase in affinity for DNA (Hagman & Grosschedl, 1992; Lim et al., 1992; Nye et al., 1992; Waslyk et al., 1992; Fisher et al., 1994; Petersen et al., 1995; Jonsen et al., 1996). Several natural variants of Ets-1, differing in either the amino or carboxy sequences flanking the ETS domain, also display enhanced DNA binding. An alternatively spliced isoform of Ets-1, lacking exon VII, binds to DNA with high affinity (Waslyk et al., 1992; Fisher et al., 1994). This exon encodes the amino-terminal inhibitory sequence. The oncogenic viral form of Ets-1, v-Ets, contains a 16-amino acid substitution within the carboxy-terminal inhibitory sequence that also results in increased DNA-binding affinity (Leprince et al., 1983, 1992, 1993; Nunn et al., 1983; Nunn & Hunter, 1989; Hagman & Grosschedl, 1992; Lim et al., 1992; Hahn & Waslyk, 1994).

A current model for Ets-1 auto-inhibition proposes that the inhibitory regions interact and together disrupt DNA binding by the intervening ETS domain (Jonsen et al., 1996). To explore the structural basis of this intramolecular repression, we have characterized an inhibited deletion mutant of Ets-1 using NMR spectroscopy. This minimal-sized protein fragment, denoted as Ets-1ΔN280, was identified by partial trypsin proteolysis of native Ets-1 (Jonsen et al., 1996). Ets-1ΔN280 contains residues 280–440 of Ets-1, including the ETS domain and both flanking inhibitory regions. Quantitative binding studies demonstrate that Ets-1ΔN280 and full-length Ets-1 are inhibited to a similar degree and make identical contacts to DNA (Petersen et al., 1995; J.M. Petersen, Q.-P. Xu, B.J. Graves, unpubl. data).

The main-chain ^1H , ^{13}C , and ^{15}N resonances of Ets-1ΔN280 were assigned and its secondary structure determined using chemical shift, NOE, J coupling, and amide hydrogen exchange information. In addition to the three α -helices and four β -strands in the wHTH ETS domain, Ets-1ΔN280 is comprised of two α -helices and an unstructured region in the amino-terminal inhibitory sequence and one α -helix in the carboxy-terminal sequence. A comparison of the backbone chemical shifts of Ets-1ΔN280 were made with those of a high-affinity DNA-binding fragment, Ets-1ΔN331, that lacks the amino-terminal inhibitory residues (Donaldson et al., 1994; Petersen et al., 1995). The spectral differences demonstrate that the amino- and

carboxy-terminal inhibitory sequences are structurally coupled and that they interact with the ETS domain. This provides an explanation for the observation that both sequences are required for the repression of DNA binding and leads to a more explicit structural model to account for the mechanism of Ets-1 auto-inhibition.

Results

Main-chain resonance assignments

Ets-1ΔN280 is a deletion mutant of murine Ets-1, composed of the 51-residue amino-terminal inhibitory region (Val 280–Thr 330), the ETS domain (Gly 331–Val 415), and the 25-residue carboxy-terminal inhibitory sequence (Cys 416–Asp 440). Asp 440 is the native carboxy-terminal residue of Ets-1. Using the methods described below, complete assignments were obtained for 139 of 150 expected backbone ^{15}NH signals in the ^1H - ^{15}N HSQC spectrum of Ets-1ΔN280 (Table 1; Fig. 1). These include all amide signals except those of Ser 282, Asp 284, Glu 289, Asp 290, Asn 297, His 298, Ile 321, Asp 398, Lys 399, Gly 407, and Asp 417. Each resolved H^N signal has been accounted for, and thus the unassigned resonances are either in the extensively overlapped central region of the ^1H - ^{15}N HSQC spectrum or display low intensity. Four tryptophan $^{15}\text{N}^\epsilon\text{H}$ signals were identified from characteristic ^1H and ^{15}N chemical shifts and NOE connectivities. Nine $^{15}\text{NH}_2$ signals expected for the four glutamine and five asparagine residues were identified but not completely assigned. The H^ϵ from the arginines exchange too rapidly with solvent at pH 7.1 and 32 °C to be observed. The completeness of backbone ^{15}N and H^N assignment achieved was 93%, despite many overlapping signals of variable intensity in the ^1H - ^{15}N HSQC spectrum of this protein.

Absolutely key to the initial stage of the assignment strategy were ^1H - ^{15}N HSQC spectra of selectively [α - ^{15}N]-Ala-, -Asp- and -Asn-, -Leu-, -Lys-, -Tyr-, or -Val-labeled Ets-1ΔN280 proteins, as shown in Figure 2. These spectra provided unambiguous markers in the primary structure for tracing the backbone assignments and helped to identify confidently peaks in the extensively overlapped regions of the spectrum of the uniformly ^{15}N -enriched protein.

After analysis of these selectively labeled proteins, 3D triple resonance HNCACB (Wittekind & Mueller, 1993), CBCA(CO)NH (Grzesiek & Bax, 1992), CBCACO(CA)HA (Kay, 1993), and HNCO (Ikura et al., 1990) experiments were used to assign sequentially the backbone ^{15}N , H^N , C^α , H^α , C' , and side-chain C^β resonances of ^{13}C / ^{15}N -enriched Ets-1ΔN280. The HNCACB correlates both the C^α and C^β frequencies of residue (*i*) with the intraresidue ^{15}N and H^N frequencies via the one bond $^1\text{J}_{\text{C}\alpha\text{N}}$ coupling constant (~11 Hz) and the ^{15}N and H^N for the residue (*i* + 1) via the two bond $^2\text{J}_{\text{C}\alpha\text{N}}$ coupling constant (~7 Hz). In contrast, the CBCA(CO)NH associates the C^α and C^β frequencies of residue (*i*) with the ^{15}N and H^N for the residue (*i* + 1). Using this approach, combined with selective α - ^{15}N -labeling and the diagnostic C^α , C^β , and, to a lesser extent, ^{15}N chemical shifts for the different amino acids, we were able to identify and assign the ^{15}N , H^N , C^α , and C^β frequencies for most residues in Ets-1ΔN280. The HNCO spectrum was then used to correlate the ^{15}N and H^N frequencies of residue (*i*) with the C' signal of residue (*i* – 1), and the CBCACO(CA)HA spectrum was used to group the intraresidue C^α , C^β , H^α , and C'

Table 1. NMR resonance assignments for backbone nuclei in Ets-1ΔN280 at pH 7.0 and 32 °C^a

Residue	¹⁵ N (¹ H ^N)	¹³ C ^α (¹ H ^α)	¹³ C ^β (¹ H ^β)	¹³ C'	Residue	¹⁵ N (¹ H ^N)	¹³ C ^α (¹ H ^α)	¹³ C ^β (¹ H ^β)	¹³ C'
V280 ^b	126.2 (8.14)	63.8	35.2		L342	118.2 (6.89)	58.0 (3.84)	41.9 (1.72)	177.8
P281					E343	123.0 (7.60)	59.6 (4.10)	29.0	178.9
S282		61.2 (4.20)	62.8	175.0	L344	118.8 (7.70)	58.1 (3.96)	41.9	180.7
Y283	123.0 (7.93)				L345	116.9 (8.09)	56.5 (3.65)	42.3	178.6
D284		54.4 (4.58)	41.4	176.0	T346	111.4 (7.81)	60.3 (4.85)	67.9 (4.38)	178.0
S285	117.0 (8.03)	58.5 (4.33)	63.8	174.1	D347	125.5 (7.24)	52.2 (4.86)	43.2 (3.41 ^c)	176.6
F286	123.2 (8.15)	57.8 (4.58)	39.4	175.2	K348	126.5 (8.88)	59.8 (3.94)	32.9	178.1
D287	123.0 (8.12)	54.3	41.2	176.0	S349	115.2 (8.63)	60.8 (4.44)	63.4 (4.16)	176.4
Y288	123.0 (8.07)				C350	121.8 (8.16)	59.4 (4.45)	27.9	174.6
E289		56.5	30.6		Q351	119.7 (7.08)	58.4 (4.34)	28.2	176.8
D290		54.4 (4.58)	41.2	175.7	S352	114.2 (8.24)	60.3 (4.26)	62.8 (3.83)	174.8
Y291	121.5 (7.82)	58.3	38.7		F353	117.4 (7.54)	56.2 (5.11)	41.4 (3.20, 3.31)	174.7
P292		63.6 (4.38)	31.6	176.4	I354	124.8 (7.74)	60.4 (5.19)	39.6	180.1
A293	125.1 (8.08)	52.6 (4.38)	19.3	177.3	S355	118.8 (8.54)	56.9 (4.82)	65.5 (3.95, 4.35)	174.1
A294	124.0 (8.10)	52.4 (4.38)	19.6	177.2	W356	125.0 (8.98)	56.6 (5.28)	29.7	177.9
L295	123.2 (8.05)	56.1	41.8		T357	113.1 (8.55)	62.8 (4.35)	69.1 (4.35)	176.8
P296					G358	110.9 (8.76)	44.4 (3.82, 4.23)		172.0
N297					D359	123.9 (7.72)	51.7 (4.90)	41.0 (2.43, 2.87)	175.7
H298					G360	114.5 (8.85)	47.5 (3.21, 3.76)		175.1
K299	122.0 (7.78)				W361	128.7 (9.32)	55.1 (5.57)	30.2 (3.68)	176.3
P300		63.2 (4.40)	32.0	176.4	E362	125.1 (8.38)	56.7 (5.41)	31.6	176.1
K301	122.2 (8.40)	56.7 (4.36)	33.2	177.5	F363	128.9 (10.30)	56.5 (5.79)	43.9	179.1
G302	112.5 (8.39)	45.4 (4.14, 4.69)			K364	120.8 (9.64)	53.7 (5.48)	37.4 (1.71)	175.2
T303	112.7 (8.43)	60.7 (4.82)	72.3	175.9	L365	125.7 (8.90)	53.6 (4.95)	41.6 (2.16)	174.9
F304	123.9 (8.61)	61.8 (3.26)	39.9	175.8	S366	121.9 (7.63)	60.7 (4.35)	62.7 (3.79)	175.2
K305	119.4 (7.93)	59.7 (3.73)	32.6	178.4	D367	118.5 (8.00)	51.2 (5.03)	41.8 (2.61, 3.23)	173.4
D306	119.1 (7.32)	56.8 (4.31)	41.4 (2.78)	177.2	P368		65.1 (3.89)	32.2	177.9
Y307	123.9 (7.79)	60.5 (4.22)	39.0 (2.44, 2.88)	177.5	D369	117.7 (7.80)	57.8 (4.40 ^c)	40.5 (2.71, 2.83)	178.6
V308	116.2 (7.79)	63.4 (3.61)	31.7 (1.85)	177.3	E370	124.5 (7.59)	58.1 (4.08)	28.6	178.6
R309	123.5 (7.39)	58.8 (4.02)	30.0 (1.89)	177.2	V371	119.7 (7.44)	67.9 (3.42)	31.2 (2.30)	177.4
D310	119.1 (7.92)	55.0 (4.61)	40.9 (2.61, 2.74)	176.5	A372	121.1 (8.12)	55.6 (4.08)	17.9 (1.45)	178.6
R311	121.6 (7.68)	55.8 (4.32)	30.3	176.2	R373	120.5 (8.41)	59.7 (4.03)	30.6 (2.69)	180.4
A312	126.2 (8.13)	52.3 (4.27)	19.2	177.3	R374	120.5 (8.33)	59.8 (4.04)	29.9	179.0
D313	124.1 ^c (8.16 ^c)	53.26 ^c	41.75 ^c (4.58 ^c)	176.6 ^c	W375	125.7 (8.58)	58.4 (4.05)	30.7	176.8
L314	122.7 (7.95)	55.5 (4.34)	41.9	177.2	G376	106.6 (8.64)	48.1 (3.29, 3.93)		176.5
N315	119.9 (8.12)	53.4 (4.56)	39.4 (2.79, 2.95)	175.6	K377	122.5 (7.88)	58.8 (4.04)	32.3 (1.92)	179.3
K316	122.7 (8.14)	56.8 (4.20)	30.7	175.8	R378	121.1 (7.70)	56.7 (4.33)	29.1	177.4
D317	122.3 (8.15)	56.6 (4.46)	40.1	177.6	K379	116.3 (7.38)	52.8 (3.98)	30.4	175.3
K318	116.2 ^c (7.30 ^c)	54.5 ^c (4.36 ^c)	32.9 ^c		N380	119.0 (7.49)	54.2 (4.24)	36.8 (2.66, 3.10)	173.9
P319		62.8 (4.55)	31.9	176.1	K381	119.7 (8.62)	52.6 (4.78)	33.9	174.2
V320	121.9 (8.02)	63.0	32.5		P382		64.1 (4.30)	32.3	177.8
I321					K383	118.6 (8.52)	55.4 (4.33)	30.7	176.6
P322					M384	122.6 (7.82)	55.8 (4.31)	30.4	174.1
A323		55.3 (3.92)	17.6	179.4	N385	122.7 (7.36)	51.6 (4.83)	39.9	175.3
A324	119.6 (9.29)	54.9 (3.98)	18.0 (1.43)	180.9	Y386	122.4 (9.56)	62.3 (4.16)	37.6 (3.02)	176.4
A325	121.3 (7.03)	54.7 (4.55)	18.7	179.6	E387	124.3 (8.48)	60.4 (3.78)	28.7 (2.08, 2.34)	179.6
L326	122.9 (8.07)	57.8 (4.07)	41.5	179.2	K388	120.9 (8.23)	59.8 (4.02)	33.7	180.1
A327	125.4 (8.79)	55.4 (4.10)	17.8 (1.40)	180.6	L389	126.1 (8.47)	59.2 (4.02)	42.5 (1.89, 2.04)	178.8
G328	107.8 (7.88)	47.1 (3.96, 4.07)			S390	116.1 (8.90)	62.0 (3.85)	62.0	176.8
Y329	124.2 (8.38)	60.3 (3.88)	39.3 (2.80, 3.02)	176.7	R391	124.7 (7.59)	59.7 (4.04)	29.8	179.1
T330	107.1 (8.06)	62.6 (3.94)	70.4 (3.79)	175.5	G392	110.4 (7.75)	46.7 (3.53, 3.65)		
G331	112.2 (7.74)	46.5 (4.02, 4.02)			L393	121.8 (7.88)	58.2 (3.99)	40.9	178.6
S332	115.4 (8.26)	59.7 (4.31)	64.3 (3.88)	174.4	R394	120.7 (7.86)	58.8 (3.51)	29.6	178.8
G333	113.3 (8.24)	44.3 (4.29, 3.66)			Y395	122.1 (7.42)	61.0 (4.27)	38.0	177.0
P334		62.3 (4.42)	32.7	176.7	Y396	115.9 (7.53)	58.9 (4.36)	37.9	178.3
I335	120.7 (8.14)	62.3 (4.64)	39.6 (1.66)	176.0	Y397	125.5 (8.27)	58.9 (5.38 ^c)	37.1	
Q336	124.8 (8.26)	52.8 (4.88)	32.9 (1.42)	177.8	D398				
L337	127.7 (9.46)	58.7 (2.93)	39.7 (2.10)	178.2	K399		54.5 (4.33)	32.4	175.3
W338	115.6 (7.91)	60.2 (3.99)	27.0	175.8	N400	116.8 (8.14)	54.9 (4.08)	36.7	173.1
Q339	119.3 (5.82)	57.1 (3.23)	26.8 (2.26)	177.8	I401	115.2 (8.09)	62.8 (4.10)	39.7	176.4
F340	122.0 (7.86)	61.2 (4.11)	40.3	176.3	I402	119.2 (6.96)	59.8 (4.97)	43.4	174.1
L341	117.8 (8.30)	58.1 (3.51)	40.7 (1.89)	177.8	H403	125.2 (9.02)	53.2 (5.15)	35.4 (2.97, 3.13)	174.4

(continued)

Table 1. Continued

Residue	^{15}N ($^1\text{H}^\alpha$)	$^{13}\text{C}^\alpha$ ($^1\text{H}^\alpha$)	$^{13}\text{C}^\beta$ ($^1\text{H}^\beta$)	$^{13}\text{C}'$	Residue	^{15}N ($^1\text{H}^\alpha$)	$^{13}\text{C}^\alpha$ ($^1\text{H}^\alpha$)	$^{13}\text{C}^\beta$ ($^1\text{H}^\beta$)	$^{13}\text{C}'$
K404	125.7 (8.14)	56.2 (4.28)	34.0	176.3	G423	106.9 (8.25)	45.4 (3.85, 4.17)		173.4
T405	127.0 (8.16)	63.8 (4.06)	69.0	182.2	Y424	117.4 (6.78)	57.0 (5.03)	42.7 (3.21, 2.39)	175.3
A406	108.5 (8.68)	53.5 (4.06)	18.7 (1.40)		T425	111.1 (8.21)	59.0 (4.64)	68.2	173.3
G407		45.0		173.5	P426		65.1 (2.59)	29.6	176.8
K408	119.5 (7.15)	54.1 (4.66)	35.6	175.0	E427	114.4 (8.15)	60.4 (3.57)	28.4	179.9
R409	123.5 (8.29)				E428	122.3 (7.62)	58.9 (4.00)	30.8 (2.13, 2.38)	179.4
Y410	118.7 (8.48)	57.4 (4.10)	39.4	173.5	L429	121.8 (7.40)	57.6 (3.99)	41.5	178.9
V411	119.7 (7.06)	61.7 (4.87)	33.6 (1.49 ^c)	174.6	H430	119.3 (8.87)	57.5 (4.13)	31.1	178.6
Y412	128.7 (8.78)	55.9 (4.93)	43.4	172.8	A431	121.4 (7.71)	54.7 (4.35)	17.9 (1.56)	181.0
R413	118.9 (9.11)	55.5 (5.25)	36.2	177.2	M432	119.0 (7.73)	58.6 (4.23)	33.8 (2.26, 2.68)	177.3
F414	125.7 (8.06)	60.0 (5.17)	40.1	176.4	L433	119.8 (7.62)	54.0 (4.39)	42.5 (1.90)	175.2
V415	117.1 (8.15)	61.3 (4.56)	31.3	175.5	D434	119.7 (7.80)	55.3 (4.43)	39.9 (2.68, 3.02)	175.3
C416	118.3 (7.29)	54.6 (4.86)	28.8 (2.79, 3.04)		V435	120.8 (8.06)	63.4 (3.91)	32.6 (1.87)	176.0
D417		53.2 (4.73)	38.3	177.1	K436	129.9 (8.40)	53.2 (4.76)	33.0 (1.74, 1.86)	174.0
L418	125.4 (7.71)	56.6 (3.80)	41.0	178.7	P437		63.2 (4.41)	32.0	176.7
Q419	122.5 8.92)	59.9 (4.60)	28.5 (2.28, 2.40)	179.8	D438	122.8 (8.39)	54.2 (4.59)	41.4 (2.63, 2.72)	175.7
S420	116.6 (7.80)	61.0 (4.21)	62.6	175.0	A439	126.3 (8.15)	52.3 (4.38)	20.0 (1.41)	176.5
L421	121.3 (7.09)	57.5 (4.45)	43.8	177.9	D440	127.1 (7.93)	56.0 (4.38)	42.4 (2.57, 2.67)	181.0
L422	114.2 (9.05)	55.9 (4.39)	43.9	178.1					

^a Chemical shifts for ^{13}C , ^{15}N , and ^1H are given in ppm. ^{13}C frequencies are referenced to an external DSS standard at 0.0 ppm. ^{15}N frequencies are referenced to an external standard of 2.9 M $^{15}\text{NH}_4\text{Cl}$ in 1 M HCl at 24.93 ppm relative to ammonia at 0.0 ppm at 25 °C. ^1H frequencies are referenced to the water signal at 4.70 ppm at 32 °C relative to DSS at 0.00 ppm.

^b A weak signal from Val 280, arising from $\Delta\text{N}280$ with incomplete N-terminal processing, was observed.

^c Tentative assignment.

signals. This served to confirm the assignments deduced from the former two experiments, as well as to identify the H^α and C' resonances of each residue in the protein. Lastly, a limited number of additional side-chain proton and carbon assignments were obtained from a HCCH-TOCSY spectrum of Ets-1 $\Delta\text{N}280$. These resonance assignments, made independently of those previously reported for Ets-1 $\Delta\text{N}331$ (Donaldson et al., 1994), are presented in Table 1.

Confirmation of the triple resonance-derived assignments was accomplished using additional NMR experiments. Through analysis of a 3D ^{15}N -separated TOCSY-HSQC and NOESY-HSQC spectra, we identified the ^{15}N , H^α , and H^β frequencies for residues having resolved H^α signals and extended the assignments to include side-chain H^β protons. Eleven proline residues in Ets-1 $\Delta\text{N}280$ broke the backbone into 12 segments that made identification of the residues preceding a proline unambig-

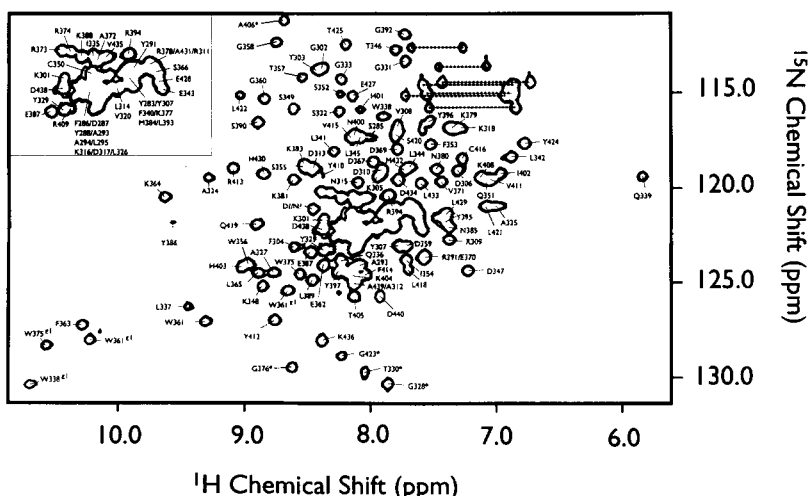


Fig. 1. ^1H - ^{15}N gradient HSQC spectrum of Ets-1 $\Delta\text{N}280$ at pH 7.10 and 32 °C showing the identities of amide ^{15}NH and tryptophan ^{15}N - ^1H correlations. Assignments of signals in the densely crowded region of the spectrum are indicated in the upper left panel. Aliased correlations are denoted by an asterisk. Dashed lines connect the pairs of $\text{N}^\delta\text{H}_2$ or $\text{N}^\epsilon\text{H}_2$ signals from asparagine and glutamine side chains, respectively.

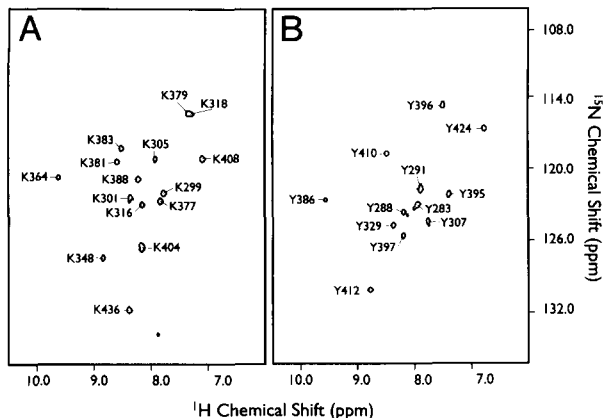


Fig. 2. ^1H - ^{15}N HSQC spectrum of selectively (A) α - ^{15}N -lysine- and (B) β - ^{15}N -tyrosine-labeled Ets-1 Δ N280 at pH 7.1 and 32 °C. ^{15}N and H^α signals are observed and assigned for all 12 tyrosine residues and for 15 of the 16 lysine residues in Ets-1 Δ N280. The use of selectively ^{15}N -labeled protein was necessary to assign the resonances in the highly overlapped region of the spectrum shown in Figure 1.

uous. To address this issue, we used a modified 2D CBCACO (CA)HA experiment to correlate only the C^β , C^α , and H^α signals for the residues preceding a proline (Olejniczak & Fesik, 1994). This helped to identify seven residues that precede prolines.

Secondary structure

After completion of the resonance assignments, we identified the regular secondary structural elements of Ets-1 Δ N280 using information from secondary chemical shifts, main-chain NOEs, $^3\text{J}_{\text{HN-H}\alpha}$ scalar coupling constants, and amide hydrogen exchange rates (Fig. 3). Strong sequential $d_{\text{NN}(i,i+1)}$ NOEs, medium $d_{\alpha\text{N}(i,i+3)}$ NOEs, small $^3\text{J}_{\text{HN-H}\alpha}$ coupling constants, slowly exchanging amide protons, downfield-shifted C^α and C' frequencies (e.g., positive secondary shifts), and upfield-shifted C^β and H^α frequencies are diagnostic segments of helical structure (Wüthrich, 1986; Wishart & Sykes, 1994). In contrast, β -strands are identified by strong sequential $d_{\alpha\text{N}(i,i+1)}$ NOEs, weak sequential $d_{\text{NN}(i,i+1)}$ NOEs, large $^3\text{J}_{\text{HN-H}\alpha}$ coupling constants, slowly exchanging amide protons, upfield-shifted C^α and C' frequencies, and downfield-shifted C^β and H^α frequencies. Cross strand $d_{\text{NN}(i,j)}$ and $d_{\alpha\alpha(i,j)}$ NOEs reflect the pairing and alignment of extended strands within β -sheets. Due to deviations from ideal geometry, the endpoints of helices and strands are often difficult to define accurately by these criteria. Stretches of residues lacking these characteristic NMR features were assigned as loops and disordered regions.

Ets-1 Δ N280 is comprised of six distinct α -helices, defined by the data summarized in Figure 3. Two of the helices, helix H1 and helix H2, are located in the amino-terminal inhibitory region, helices (H1-H3) comprise the DNA-binding wHHTH ETS domain, and helix H4 is situated within the carboxy-terminal inhibition region. To maintain a consistent nomenclature, helices H1-H4 correspond to those previously identified in Ets-1 Δ N331 (Donaldson et al., 1994, 1996), whereas H1 and H2 designate the two helices identified in the amino-terminal inhibitory region. Helix H1 extends from Thr 303 to Asp 310 and helix H2

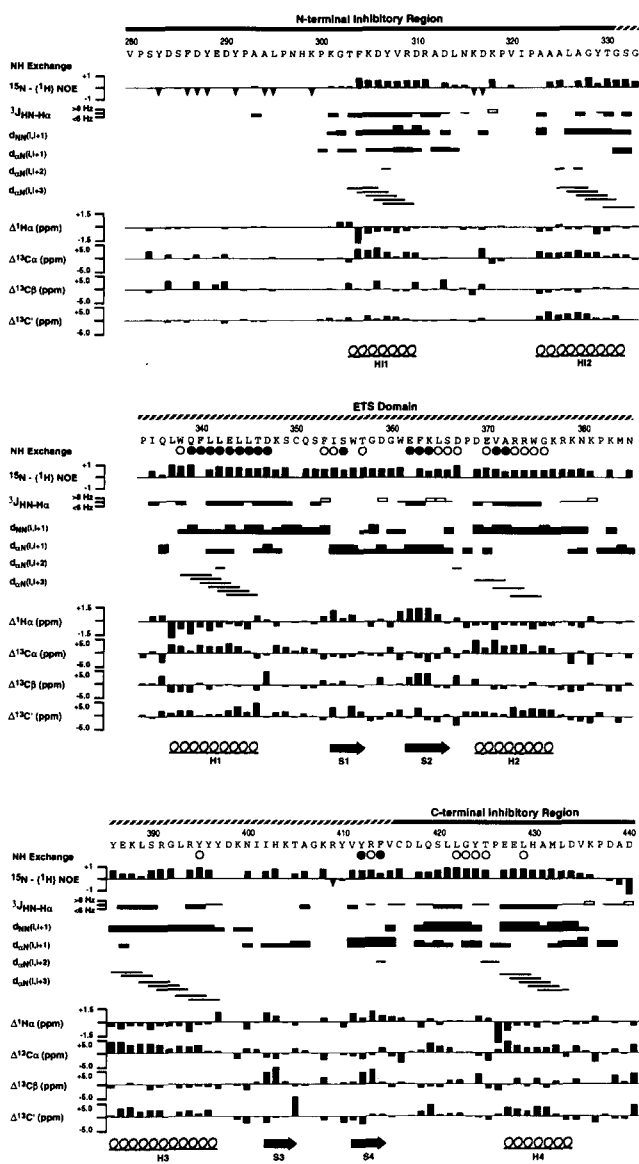


Fig. 3. Summary of amide hydrogen exchange rates, ^{15}N - $\{^1\text{H}\}$ NOE, $^3\text{J}_{\text{HN-H}\alpha}$ coupling constants, sequential and intermediate range NOE connectivities, and secondary $^1\text{H}^\alpha$, $^{13}\text{C}^\alpha$, $^{13}\text{C}^\beta$, and $^{13}\text{C}'$ chemical shifts used to determine the secondary structure of Ets-1 Δ N280. Sequences of Ets-1 Δ N280 corresponding to the amino- and carboxy-terminal inhibitory regions and the ETS domain are indicated. Locations of the six α -helices (H) and four β -strands (S) in Ets-1 Δ N280 are marked by coils and arrows, respectively. Hydrogen exchange: Filled circles indicate residues, with resolved ^{15}NH signals, that had slow amide hydrogen-deuterium exchange kinetics ($t_{1/2} > 1,000$ min), and open circles indicate those with intermediate exchange kinetics (50 min $< t_{1/2} < 1,000$ min) at pH* 7.1 and 32 °C. Steady-state ^{15}N - $\{^1\text{H}\}$ NOE are calculated as $(I_{\text{noe}}/I_{\text{control}})$. Shaded boxes indicate uncertain measurements due to partial peak overlap or low signal-to-noise. Shaded, downward-pointing triangles denote residues with signals approximately nulled or inverted by the heteronuclear NOE, yet due to extensive peak overlap, could not be quantitated. $^3\text{J}_{\text{HN-H}\alpha}$: Residues with measurable $^3\text{J}_{\text{HN-H}\alpha}$ coupling constants > 8 Hz are indicated with an open box, $^3\text{J}_{\text{HN-H}\alpha} < 6$ Hz with a solid box, and between these limits with a line. Homonuclear NOEs between H^α and H^β are labeled as $d_{\text{NN}(i,i+1)}$, $d_{\alpha\text{N}(i,i+1)}$, $d_{\alpha\text{N}(i,i+2)}$, and $d_{\alpha\text{N}(i,i+3)}$. Relative NOE strength (weak/medium/strong) is reflected by the bar thickness ($t_{\text{mix}} = 100$ ms). Main-chain $^1\text{H}^\alpha$, $^{13}\text{C}^\alpha$, $^{13}\text{C}^\beta$, and $^{13}\text{C}'$ chemical shifts are plotted as the difference from the corresponding random coil values (observed - random coil shift; Wishart et al., 1992; Wishart & Sykes, 1994).

from Ala 323 to Ser 332. No slowly exchanging amide hydrogens are observed in helix H1 or helix H2 at 32 °C and pH* 7.1. However, under these stringent conditions, the lifetime of an amide hydrogen in an unstructured polypeptide is short (e.g., millisecond timescale; Bai et al., 1993). Helix H1 extends from residues Leu 337 to Thr 346 and contains 10 slowly exchanging amide hydrogens. Helix H2 is comprised of residues Asp 369–Lys 377 and contains seven slowly exchanging amide hydrogens. Proline 368 defines the amino-terminal side of this helix. Helix H3 includes residues Tyr 386–Tyr 397 and contains a single slowly exchanging amide hydrogen. The final helix, H4, extends from Glu 427 to Asp 434 in the carboxy-terminal inhibitory sequence and also contains a single slowly exchanging amide hydrogen.

Five of the α -helices in Ets-1 Δ N280 are amphipathic and one, helix H12, is primarily hydrophobic. Modeling helix H11 as a right-handed α -helix with standard geometry shows a small hydrophobic face formed with Phe 304, Tyr 307, and Val 308 and a more extensive hydrophilic surface formed with residues Thr 303, Lys 305, Asp 306, Arg 309, and Asp 310. In contrast, helix H12 is comprised primarily of hydrophobic alanine and leucine residues and contains a single hydrophilic serine 332 at its carboxy terminus (see Fig. 8). Helices H1, H2, H3, and H4 show varying degrees of amphipathicity, consistent with their packing arrangement in the intact protein (Donaldson et al., 1996).

A four-stranded antiparallel β -sheet, diagrammed in Figure 4, is observed in Ets-1 Δ N280. This β -sheet can be described as being formed by two β -hairpins, positioned in a side-by-side arrangement. The long-range $d_{\alpha N}$, d_{NN} , and $d_{\alpha \alpha}$ NOEs observed in the 2D 1H - 1H NOESY and 3D ^{15}N -separated NOESY-HSQC spectra of Ets-1 Δ N280 provide unambiguous evidence for the (+1, +2x, -1) alignment of the four strands in the order S1-S2-S4-S3 (Richardson, 1981). Helices H2 and H3, which form the HTH motif, lie between strands S2 and S3. One of the β -hairpins extends from Ile 354 to Ser 366 and contains a four-residue turn. The other β -hairpin is formed by Ile 402-Phe 414, with an intervening five-amino acid turn. The β -sheet is distinctly amphipathic, with one face comprised of the hydrophobic side chains of Ile 354, Trp 356, Trp 361, Phe 363, and Leu 365 from strands S1 and S2, and Ile 402, Ala 406, Tyr 410, Tyr 412, and Phe 414 from strands S3 and S4. The opposite side of the sheet is comprised mostly of hydrophilic side chains, including Ser 355, Thr 357, Glu 362, Lys 364, and Ser 366 from S1 and S2, and His 403, Thr 405, and Arg 413 from S3 and S4. Finally, the turns in each β -hairpin are comprised of many hydrophilic residues.

Several segments of the backbone of Ets-1 Δ N280 do not adopt a regular secondary structure and appear to exist in disordered conformations. The first ~20 residues of the protein from V280 to P300 have many degenerate ^{15}N and H^N signals (Fig. 1). Indeed, 6 of the 10 amides in Ets-1 Δ N280 with unassigned resonances are within this sequence. The C^α , C^β , C' , and H^α resonances assigned for the N-terminal residues of Ets-1 Δ N280 show relatively small deviations from the expected "random coil" chemical shifts based on amino acids in model peptides (Fig. 3). Although extensive H^N and ^{15}N degeneracy prevented the confident identification of NOEs to many of these H^N signals, no evidence for any regular structure in this region was observed in the 3D ^{15}N -separated NOESY-HSQC spectrum of Ets-1 Δ N280. Four prolines, Pro 281, Pro 292, Pro 296, and Pro 300, are contained in this amino-terminal sequence and undoubtedly contribute to the lack of regular secondary struc-

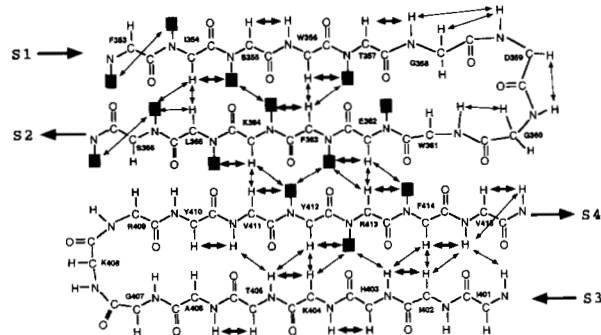


Fig. 4. Schematic diagram of the four-stranded antiparallel β -sheet in Ets-1 Δ N280. Observed NOEs between H^N and H^α , diagnostic of β -sheet topology, are indicated by arrows. Strong sequential $d_{\alpha N(i,i+1)}$ NOEs are shown with heavy arrows. Amide protons with intermediate or slow hydrogen-deuteron exchange kinetics are shaded ($t_{1/2} > 50$ min, pH 7.1, 32 °C). Directions of the four strands, S1–S4, that comprise the antiparallel β -sheet are indicated. Stereochemistries of the two hairpin turns have not been determined.

ture. Similar behavior is observed for the 12-amino acid loop between helices H11 and H12, containing prolines Pro 319 and Pro 322.

Although it is possible that the residues preceding and following helix H11 in the amino-terminal inhibitory region of Ets-1 Δ N280 adopt static structures with backbone dihedral angles leading to apparent "random coil" chemical shifts, it is much more likely that these two sequences are conformationally disordered and undergo motions resulting in chemical shift averaging. This is consistent with the observed lack of protection from hydrogen exchange for the amides within these regions. Also, in sharp contrast to the regions of regular secondary structure in Ets-1 Δ N280, the residues near the amino-terminus of Ets-1 Δ N280 and between helices H11 and H12 show significant ^{15}N -{ 1H } heteronuclear NOEs. This indicates a high degree of internal mobility (Fig. 3; Kay et al., 1989).

On this note, several regions of Ets-1 Δ N280 display very different effective NMR correlation times. We have observed up to ~10-fold variation in signal intensity for nuclei located in different regions of the protein. For instance, the signals from nuclei in residues Asp 434–Asp 440 at the extreme carboxy-terminus of Ets-1 Δ N280 are considerably sharper than those from the remainder of the protein. In addition, these residues show large negative ^{15}N -{ 1H } heteronuclear NOEs. Together, this demonstrates that the carboxy-terminus undergoes fast local motions relative to the overall tumbling of the molecule. In contrast, signals from nuclei located in the loop from Gly 333 to Ile 335 that connects helix H12 and H11, the loop from Asp 398 to Ile 401, connecting helix H3 with β -strand S3, and the sequence Ala 406–Tyr 410 that links strands S3 and S4, are weak or are not observed in a 1H - ^{15}N HSQC spectrum. This may reflect internal motions in these regions on the intermediate time-scale that contribute to line broadening.

Discussion

Secondary structure of Ets-1 Δ N280: A wHTH motif flanked by helical inhibitory regions

Ets-1 Δ N280 is an amino-terminal deletion mutant of murine Ets-1 that retains the low-affinity DNA-binding properties ex-

hibited by full-length Ets-1. This fragment provides a model system for probing the structural origins of auto-inhibition. Using NMR spectroscopy, we have determined the secondary structure of Ets-1 Δ N280 (Fig. 3). At the core of Ets-1 Δ N280 is the previously identified wHTH ETS domain (Donaldson et al., 1994, 1996; Liang et al., 1994a, 1994b). Flanking the ETS domain is helix H4 in the carboxy-terminal inhibitory region and two helices, H1 and H12, in the amino-terminal inhibitory region. Based on NMR criteria, the helical content of Ets-1 Δ N280 is approximately 35%, which is similar to that observed previously for Ets-1 Δ N331 (Donaldson et al., 1994). This is consistent with CD measurements showing that Ets-1 Δ N280 and Ets-1 Δ N331 have similar mean residue molar ellipticities [Θ] at 222 nm (Petersen et al., 1995).

Comparison of Ets-1 Δ N280 and Ets-1 Δ N331: Evidence for direct interaction of the amino- and carboxy-terminal inhibitory regions

Key structural information regarding the mechanism of intramolecular inhibition is provided by a comparison of Ets-1 Δ N280 and Ets-1 Δ N331. This latter protein is a 110-residue deletion mutant of murine Ets-1 containing only the ETS domain and the 25-residue carboxy-terminal inhibitory region. The 3D structure of this protein has been determined by NMR methods (Fig. 6; Donaldson et al., 1994, 1996). Ets-1 Δ N331 lacks the amino-terminal inhibitory sequence and therefore binds to specific Ets-1 recognition sequences with approximately 15-fold higher affinity than either Ets-1 Δ N280 or native Ets-1 (Jonsen et al., 1996; Petersen et al., 1995).

The locations and topological arrangement of the four α -helices and four β -strands formed by residues 331–440 in the repressed (Ets-1 Δ N280) and activated (Ets-1 Δ N331) deletion mutants of Ets-1 are very similar (compare Figs. 3 and 4 with the corresponding figures in Donaldson et al. [1994]). Therefore, the amino-terminal inhibitory region does not change the secondary structure of the ETS domain or the carboxy-terminal inhibitory region. This implies that the corresponding residues of Ets-1 Δ N280 and Ets-1 Δ N331 also adopt the same tertiary wHTH fold. Consistent with this conclusion is the observation that these two proteins bind specifically to the same Ets-1 promoter sequences and show identical patterns of DNA contacts (Petersen et al., 1995; J.M. Petersen, Q.-P. Xu, & B.J. Graves, unpubl. data).

To map the interactions between residues of the amino-terminal inhibitory region with those in the remainder of Ets-1 Δ N280, we examined the chemical shift differences between corresponding main-chain ^{15}N and H^{N} nuclei in Ets-1 Δ N280 and Ets-1 Δ N331 (Figs. 5, 6). Because the chemical shift of a nucleus is highly dependent upon its structural environment, shift perturbations are an exquisitely sensitive monitor of conformation changes. Large chemical shift differences between Ets-1 Δ N280 and Ets-1 Δ N331 (e.g., $|\Delta\delta| > 0.25$ ppm and 1.0 ppm for H^{N} and ^{15}N , respectively) are observed for backbone nuclei clustered in several regions of the proteins. These include helix H1 and the sequence immediately amino-terminal to this helix, the carboxy-terminal end of helix H3, β -strand S3, and helix H4, and the loop linking this helix to the β -sheet. The spectral differences show that the presence of the amino-terminal inhibitory region structurally perturbs these residues in Ets-1 Δ N280 relative to Ets-1 Δ N331. In contrast, nuclei from residues in

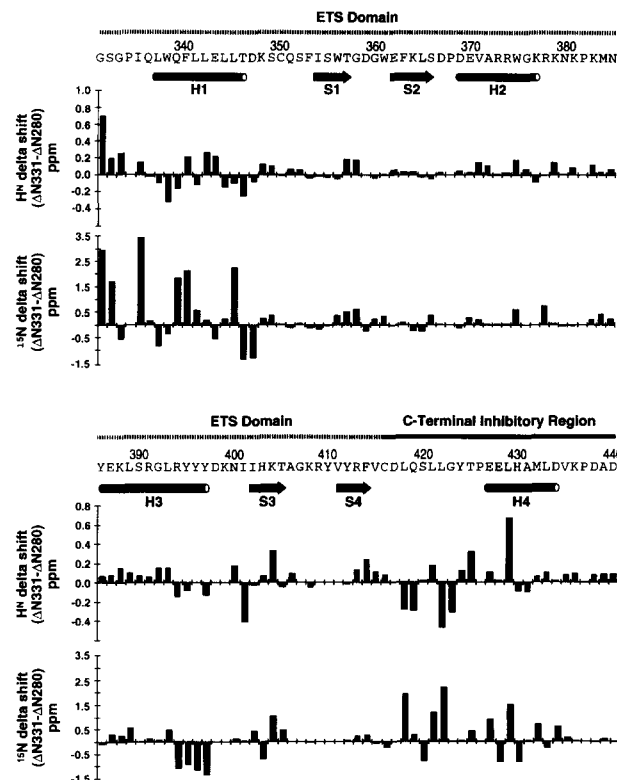


Fig. 5. Histogram showing the differences in chemical shifts for the H^{N} and ^{15}N signals from corresponding residues in Ets-1 Δ N280 and Ets-1 Δ N331. α -Helices and β -strands in the DNA-binding ETS domain and carboxy-terminal inhibitory region are shown by cylinders and arrows, respectively. Pronounced chemical shift differences observed for residues clustered in several regions, including helices H1 and H4, reflect structural perturbations due to the presence of the amino-terminal inhibitory sequence in Ets-1 Δ N280. Average shift differences (and standard deviations) are 0.03 (0.16) ppm and 0.18 (0.78) ppm for all H^{N} and ^{15}N , respectively.

β -strand S1 through the amino-terminal half of helix H3, including the HTH motif, have similar resonance frequencies, and thus similar structural environments, in the two Ets-1 fragments.

The most striking conclusion from this comparison is that significant changes in the resonance frequencies from many residues in the carboxy-terminal region, as well as helix H1 of the ETS domain, arise from the presence of the amino-terminal inhibitory sequence in Ets-1 Δ N280. This indicates that the amino- and carboxy-terminal inhibitory regions are indeed structurally coupled with one another and with the ETS domain. When the shift differences are mapped on the 3D model of Ets-1 Δ N331, a plausible reason for the observed perturbations becomes apparent (Fig. 6). Helices H1 and H4 are folded against one another in an antiparallel fashion and lie across the β -sheet scaffold of the ETS domain. Structural elements from the amino-terminal inhibitory sequence could pack upon the surface formed by H1 and H4, thus accounting for the pronounced spectral changes observed for the residues forming these helices. Because the secondary structures of Ets-1 Δ N280 and Ets-1 Δ N331 are similar, we propose that the perturbations of the chemical shifts of these residues are caused by direct interactions with the amino-terminal inhibitory sequence. The additional chemical shift perturbations observed for nuclei in the β -sheet,

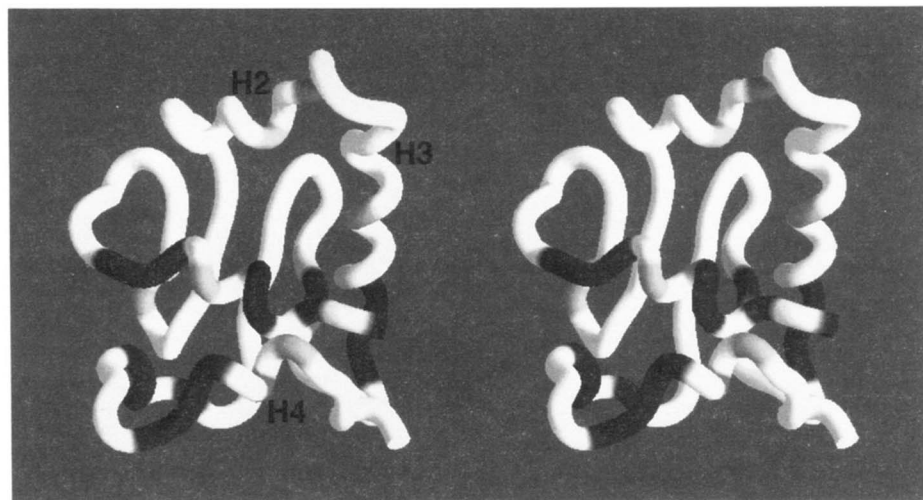


Fig. 6. Stereo view mapping the spectral perturbations due to the presence of the amino-terminal inhibitory sequence on residues Ile 335 to Asp 440 in the 3D solution structure of Ets-1ΔN331 (Donaldson et al., 1996). This high-affinity deletion mutant of Ets-1 is composed of the ETS domain and the carboxy-terminal inhibitory region, which includes helix H4. Absolute values of the differences in the amide ^{15}N chemical shifts between Ets-1ΔN331 and Ets-1ΔN280 are presented on a gray scale from light (no change; $|\Delta\delta| = 0.0 \text{ ppm}$) to dark ($|\Delta\delta|_{\max} = 3.4 \text{ ppm}$). Shift perturbations indicate that the amino-terminal inhibitory region packs on the surface formed by helix H1 of the ETS domain and helix H4 of the carboxy-terminal inhibitory region. The figure was generated using the program GRASP (Nicholls et al., 1991).

the end of helix H3, and the loop before helix H4 are attributed to structural changes propagated through the residues on the surface formed by helices H1 and H4.

Thermodynamic stability measurements of the Ets-1 deletion mutants further indicate that the amino-terminal inhibitory region interacts with the ETS domain and the carboxy-terminal residues. Ets-1ΔN280 exhibits a single sharp transition in its thermal denaturation curve with an apparent T_m of $\sim 54^\circ\text{C}$ at pH 6.3 as monitored by CD. In contrast, the apparent T_m for Ets-1ΔN331 is $\sim 45^\circ\text{C}$ under the same conditions (L.W. Donaldson, unpubl. data). These results imply that the amino-terminal inhibitory region stabilizes the structure of Ets-1ΔN280 and support the conclusion that the inhibitory regions are cooperatively folded with the ETS domain to form a single structural domain.

Structural model for Ets-1ΔN280: A helical bundle interfaced with the ETS domain

A model for the inhibition “module” of Ets-1ΔN280 invokes packing of helices HI1 and HI2 on helices H1 and H4 to form a helical bundle. This bundle folds along one side of the ETS domain with H1 shared between the inhibitory module and the ETS domain as a common secondary structural element. The helix(H2)-turn-helix(H3) DNA-binding motif is not contacted directly by HI1 or HI2 from the amino-terminal inhibitory region (Figs. 5, 6). Helices H1 and H4 are antiparallel in the 3D structure of Ets-1ΔN331 and are undoubtedly arranged similarly in Ets-1ΔN280 (Fig. 6). Helices HI2 and H1 are separated by only four residues and thus are most probably packed in an antiparallel fashion. Although we have not determined the orientation of helices HI1 and HI2, the predominantly hydrophobic helix HI2 should be in a buried environment to minimize solvent accessibility, whereas the amphipathic helix HI1 could be located on the surface of the protein (Fig. 8). The 12-residue

loop between these two provides significant conformational freedom such that HI1 could lie parallel or antiparallel to HI2. The disordered residues at the amino-terminus of Ets-1ΔN280 are not expected to contribute to the structure of the inhibitory helical bundle. Consistent with this conclusion is the recent finding that Ets-1ΔN301, which lacks residues 280–300, is inhibited to the same degree as Ets-1ΔN280 (N. Heaps, L.W. Donaldson, & B.J. Graves, unpubl. data).

Structural model for the auto-inhibition of Ets-1

NMR analysis of Ets-1ΔN280 provides four key findings relevant to the phenomenon of Ets-1 auto-inhibition of DNA binding. First, the secondary structural elements of the amino-terminal inhibitory region are identified. Second, structural coupling between the amino- and carboxy-terminal inhibitory regions is demonstrated. Third, evidence for coupling between both inhibitory regions and the ETS domain is presented. Finally, the position of the inhibitory regions with respect to the DNA-binding HTH motif is described.

The significance of these new findings is best understood within the context of the model of inhibition presented in Figure 7. In this figure the proposed helical bundle that constitutes the inhibitory module (HI1-HI2-H1-H4) is illustrated schematically. The HTH and β -sheet structures of the ETS domain are represented as a globular DNA-binding domain. The repressed fragment, Ets-1ΔN280, has the helical bundle intact. The two activated fragments, Ets-1ΔN331 (Donaldson et al., 1996; Petersen et al., 1995) and Ets-1ΔC428 (Jonsen et al., 1996), have the bundle disrupted due to the lack of either the amino- or carboxy-terminal inhibitory region, respectively. Upon DNA binding, the repressed protein Ets-1ΔN280 undergoes a conformational change involving the unfolding of HI1 (Petersen et al., 1995). This same conformation is adopted constitutively by the high-

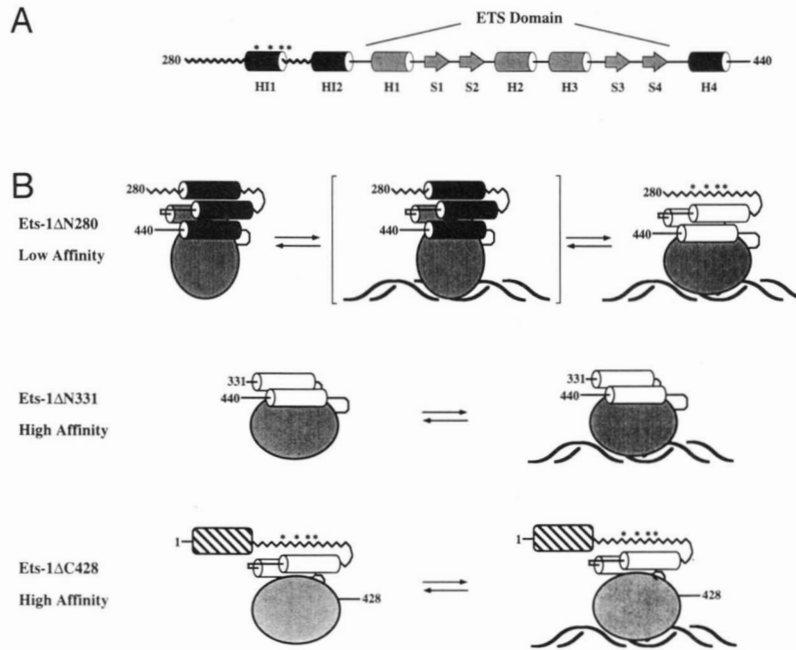


Fig. 7. A: Schematic representation of the secondary structure of Ets-1 Δ N280. α -Helices are denoted by cylinders and the β -strands by arrows. Helices H11 and H12 in the amino-terminal inhibitory region and H4 in the carboxy-terminal inhibitory region are solid black, whereas the elements of the ETS domain are shaded gray. Zig-zag line represents the conformationally disordered residues in the amino-terminal region. Asterisks (*) indicate the locations of residues showing enhanced sensitivity to proteolytic cleavage due to DNA binding by Ets-1 Δ N280 (Petersen et al., 1995) or deletion of the final 12 carboxy-terminal residues in Ets-1 (Ets-1 Δ C428; Jonsen et al., 1996). **B:** A model for intramolecular inhibition of Ets-1 DNA binding. Helices H11, H12, H1, and H4 are indicated by cylinders and the remainder of the ETS domain by a shaded oval. Possible DNA contacts include the helix(H2)-turn-helix(H3) motif as well as the N-terminus of H1 (not shown for clarity). Residues 1-279 of Ets-1 Δ C428 are represented by the hatched box. In solution, Ets-1 Δ N280, or native Ets-1, exists predominantly in a low-affinity form in which helices H11, H12, and H4 in the amino- and carboxy-terminal inhibitory regions, respectively, are packed with helix H1 of the ETS domain to form a four-helix bundle-like structure. DNA binding by Ets-1 Δ N280 is accompanied by a conformational change involving the unfolding of H11 (denoted by the changes in the shape of the oval and the shading of cylinders) (Petersen et al., 1995). Refolding of H11 restores the structure of the inhibitory module and leads to dissociation from DNA. Ets-1 Δ N331, which lacks the amino-terminal inhibitory region, and Ets-1 Δ C428, which lacks the final 12 residues of the carboxy-terminal inhibitory region, exist constitutively in this altered conformation and thus bind DNA with high affinity (Jonsen et al., 1996).

affinity fragments, Ets-1 Δ N331 and Ets-1 Δ C428 (Jonsen et al., 1996). The mechanistic basis for auto-inhibition will be presented after the supporting structural and biochemical studies for this model are summarized.

The first key feature of the model is that the amino- and carboxy-terminal inhibitory regions operate in a concerted fashion to reduce the affinity of Ets-1 for DNA. Our NMR analysis demonstrates that the chemical shifts of residues in the carboxy-terminal inhibitory region, including helix H4, are perturbed by the presence of the amino-terminal inhibitory sequence. This provides strong evidence for a direct structural coupling between the carboxy- and amino-terminal inhibitory regions. This structural coupling is supported further by the observation that deletion of the C-terminal residues of Ets-1, yielding the high-affinity mutant Ets-1 Δ C428, results in the enhanced sensitivity of the amino-terminal inhibitory region to proteolysis (Fig. 7; Jonsen et al., 1996). The intramolecular interactions between the amino- and carboxy-terminal inhibitory sequences explains how these two regions exert their effect cooperatively. Additional evidence for cooperative interactions at a functional level includes the finding that removal of both inhibitory regions generates a minimal 85-residue ETS domain polypeptide with

DNA-binding properties similar to Ets-1 Δ N331 or Ets-1 Δ C428, which have only one of the two inhibitory regions deleted (Jonsen et al., 1996).

The structural coupling of the inhibitory module to the ETS domain is an equally important feature of the model. Studies of several wHTH proteins indicate that DNA binding by Ets-1 is mediated by the HTH motif with possible additional interactions provided by the N-terminus of helix H1 and one or more loops ("wings") extending from the β -sheet scaffold (Schultz et al., 1991; Brennan, 1993; Clark et al., 1993; Liang et al., 1994b). The NMR-derived structure of Ets-1 Δ N331 shows that H1, the first helix of the ETS domain, contacts H4 in the C-terminal inhibitory region (Fig. 6; Donaldson et al., 1996). Also, the comparison of Ets-1 Δ N280 and Ets-1 Δ N331 demonstrates that helices H11 and H12 in the amino-terminal inhibitory region affect the chemical shifts of residues in H1. Helix H1 is clearly structurally linked to the HTH motif, as well as being positioned within the ETS domain to contact DNA (Liang et al., 1994b). Therefore, the connection of the amino- and carboxy-terminal inhibitory regions to helix H1 provides a structural pathway for these inhibitory sequences to influence DNA binding by the ETS domain. Importantly, these data support an

allosteric model, as diagrammed in Figure 7, in which the inhibitory module does not directly mask the helix(H2)-turn-helix(H3) DNA-binding surface of the ETS domain but rather incorporates H1 as a common element of both the DNA-binding domain and the inhibitory module.

A third feature of the model for auto-inhibition involves the coupling of DNA binding to the local unfolding of the amino-terminal inhibitory region. The identification of helix H1 within this region was a key step in understanding this observation. Two approaches independently detected a conformational change in the amino-terminal inhibitory region upon DNA binding (Petersen et al., 1995). Specifically, DNA binding by Ets-1 Δ N280 is accompanied by (1) an enhanced susceptibility to proteolysis at residues 305–312, and (2) a reduction in CD ellipticity [Θ] at 222 nm. As summarized in Figure 3, Thr 303–Asp 310 form helix H1. Unfolding of this helix accounts for the observed reduced ellipticity and enhanced protease sensitivity. This structural transition is predicted to disrupt the packing of the inhibitory module. The low-affinity proteins Ets-1 Δ N280 and native Ets-1 sample this conformation only in the presence of DNA. However, this alternative state, as detected by protease sensitivity, is constitutively adopted by the high-affinity fragment Ets-1 Δ C428, in which the C-terminal inhibitory region is deleted (Jonsen et al., 1996; Fig. 7). Thus, the model of auto-inhibition proposes that DNA binding triggers a change in the ETS domain that leads to the local unfolding of helix H1 and disruption of the inhibitory module.

The coupling of the two inhibitory regions with each other and with the ETS domain provides the structural framework for understanding Ets-1 auto-inhibition. The interactions between the amino and carboxy inhibitory regions and helix H1 of the ETS domain form an inhibitory module that compromises the interactions between Ets-1 and DNA. High-affinity binding, as seen with derepressed Ets-1 Δ N331 and Ets-1 Δ C428, results from elimination of the link between the inhibitory regions and the ETS domain. DNA binding by the low-affinity fragments, such as native Ets-1 and Ets-1 Δ N280, is accompanied by a conformational change involving the unfolding of helix H1 and disruption of the inhibitory module. Refolding of H1 promotes reassociation of the inhibitory regions and leads to dissociation from DNA. This model is consistent with the crucial finding that repressed and derepressed fragments of Ets-1 differ most dra-

matically in the dissociation rate rather than association rate of the DNA-protein complex (Jonsen et al., 1996). Refinement of this model of auto-inhibition will follow from further NMR characterization of the low- and high-affinity fragments of Ets-1 in the absence and presence of DNA.

Implication of the model to Ets-1-related polypeptides

Our NMR data also provide a structural basis for understanding how two natural variants of Ets-1 attain high-affinity interactions with DNA. An alternatively spliced isoform of Ets-1 lacking exon VII binds DNA with higher affinity than the full-length protein (Fisher et al., 1994). The two amino-terminal inhibitory helices, H1 and H2, are encoded by exon VII and consequently are absent in this Ets-1 isoform (Jorcik et al., 1991). The oncogenic form of Ets-1, v-Ets, contains a 16-amino acid substitution within the C-terminus that also results in de-repression of DNA binding (Hagman & Grosschedl, 1992; Lim et al., 1992; Hahn & Waslyk, 1994). This substitution is predicted to prevent the formation of the inhibitory helix, H4 (Donaldson et al., 1996). Therefore, the structural elements, demonstrated here to constitute the inhibitory module (H1-H2-H1-H4), are either lacking or disrupted in these high-affinity Ets-1 variants.

Ets-2, an *ets* family member closely related to Ets-1, also displays auto-inhibition of DNA binding (Hagman & Grosschedl, 1992). A comparison of the sequences of Ets-1 inhibitory elements (H1-H2-H1-H4) with the same regions in Ets-2 provides an explanation for this behavior. Alignment of the Ets-1 and Ets-2 sequences indicates that the amino acids flanking the amino- and carboxy-termini of the ETS domains of these two proteins are conserved (Fig. 8). More importantly, the charge properties and hydrophobicities of residues within the regions shown to form α -helices in Ets-1 are strikingly similar. This is readily seen on the helical wheel diagrams displayed in Figure 8. We therefore propose that DNA binding by Ets-2 also is negatively regulated by an inhibitory module similar in structure to that described for Ets-1.

Summary

Auto-inhibition coupled with its derepression by allosterically induced conformational changes is a widespread mechanism for

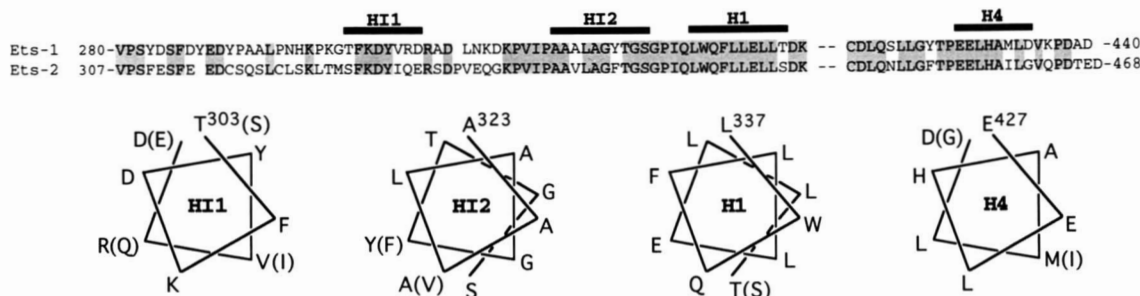


Fig. 8. Sequence alignment and helical wheel diagrams for murine Ets-1 and Ets-2. Sequence of Ets-2 (Watson et al., 1988) is aligned against the amino- and carboxy-terminal inhibitory regions and helix H1 of Ets-1, with identical residues shaded and insertions represented by open gaps. The remainder of the intervening ETS domain sequence of each protein, indicated by the two dashes between H1 and H4, is omitted for clarity. Sequences of the four helices that form the inhibitory module of Ets-1 are represented on helical wheel diagrams. Amino acids that differ at corresponding positions in Ets-2 are shown in parentheses. These substitutions are highly conservative, suggesting that sequences flanking the ETS domain of Ets-2 adopt helical structures similar to those identified in the inhibitory module of Ets-1.

the control of biological processes. In this study, we have determined the secondary structure of Ets-1 Δ N280, a low-affinity deletion mutant of Ets-1 and demonstrated that the helices in the amino- and carboxy-terminal inhibitory regions are coupled to one another and to the intervening ETS domain. This also led to the identification of an α -helix in the amino-terminal inhibitory region as the element of Ets-1 Δ N280 that undergoes a conformational change upon DNA binding. These findings provide a structural framework for interpreting data derived from extensive genetic and biochemical studies of Ets-1 auto-inhibition. A model involving intramolecular interactions and conformational change as the basis for auto-inhibition is strongly supported. In vivo, repression of Ets-1 DNA binding could be regulated by proteolysis, alternative splicing, posttranslational modifications, or protein-protein associations that influence the coupling of the amino- and carboxy-terminal inhibitory regions with the ETS domain. This study also exemplifies how the structural and functional characteristics of a transcription factor domain can be modulated by intramolecular interactions within the native protein.

Materials and methods

Recombinant protein expression and purification

The gene encoding residues 280–440 of murine Ets-1 (Ets-1 Δ N280) was expressed in *Escherichia coli* BL21 cells under the control of the T7 promoter in the plasmid pET3 (Petersen et al., 1995). Cell growth was conducted in 1–1.5-L volumes of media in a water-jacketed 3-L benchtop fermenter (Virtis, Inc.). The broth was continuously stirred at 37 °C with a constant supply of 0.2-micron filtered air and the pH was adjusted manually to 7.1 with additions of sterile 0.1 M NaOH. Cells were induced with 1 mM IPTG at OD₆₀₀ ~ 0.8, grown for an additional 4 h, and then harvested. The isolation and purification of Ets-1 Δ N280 is described elsewhere (Petersen et al., 1995). Uniformly ¹⁵N-labeled protein was prepared from cells cultured in M9 minimal media containing 1.0 g/L of 99% (¹⁵NH₄)₂SO₄ as the sole nitrogen source. Uniformly ¹⁵N- and ¹³C-enriched protein was produced from cells grown in M9 minimal media containing 1.0 g/L 99% (¹⁵NH₄)₂SO₄ and 2.0 g/L 99% [¹³C₆]glucose supplemented with 1.0 g/L 99% ¹⁵N/¹³C Isogro algal extract (Isotec, Miamisburg, Ohio) as the sole nitrogen and carbon sources. Selective [α -¹⁵N]-Ala-, -Asn- and -Asp-, -Leu-, -Lys-, -Tyr-, or -Val-labeled proteins were prepared in *E. coli* BL21 using the protocol described by McIntosh and Dahlquist (1990) and McIntosh et al. (1990). The final yield of Ets-1 Δ N280 was ~8.0 mg/L of bacterial culture, using a calculated ϵ_{280} = 3.64 × 10⁴ M⁻¹ cm⁻¹ in 6 M guanidinium hydrochloride (Edelhoch, 1967). Purity was determined to be greater than 95% for all Ets-1 Δ N280 preparations as judged by SDS-polyacrylamide electrophoresis. Equilibrium ultracentrifugation of 12 μ M Ets-1 Δ N280, in the identical buffer conditions used for NMR studies, showed that the protein migrates as a monomer with a molecular weight of 18.1 kDa. The first five residues of unlabeled Δ N280, produced in rich media, were Pro-Ser-Thr-Asp-Ser as determined by Edman sequencing. Therefore, the initial Val 280 encoded by the gene for Ets-1 Δ N280 and the amino-terminal Met from the expression plasmid were removed by posttranslational processing. However, a low level of incomplete amino-terminal process-

ing was observed for Ets-1 Δ N280 produced in minimal media, as evident by a weak signal detected from the amide of Val 280.

NMR spectroscopy

NMR experiments were performed on a Varian Unity 500 NMR spectrometer equipped with three radio frequency channels and a pulsed-field gradient accessory. ¹H and ¹³C chemical shifts were referenced to an external sample of DSS at 0.00 ppm for both nuclei, and ¹⁵N chemical shifts to an external sample of 2.9 M ¹⁵HN₄Cl in 1 M HCl at 24.94 ppm relative to liquid ammonia. NMR data were processed and analyzed using FELIX version 2.3 software (Biosym Technologies, San Diego, California). Acquisition and processing details for NMR experiments are presented in Table 2.

Solution conditions

Except when stated otherwise, identical buffer conditions (25 mM sodium phosphate, pH 7.1, 450 mM potassium chloride, 1.0 mM DTT, 0.01% sodium azide, 10% ²H₂O or 99% ²H₂O, 32 °C) were used for all Ets-1 Δ N280 samples. These conditions differ slightly from those used previously with the smaller Ets-1 fragment, Ets-1 Δ N331 (pH 6.45, 20 °C; Donaldson et al., 1994) but do not cause any appreciable changes in the chemical shifts of either protein. To partially offset the broad resonances from the nuclei in the 18-kDa Ets-1 Δ N280, an elevated temperature of 32 °C was chosen for most measurements. The stability of Ets-1 Δ N280 is highest near neutral pH, leading to the selection of pH 7.1. At this pH and temperature, the chemical exchange rate of amide hydrogens with bulk solvent is fast enough to reduce the signal intensity for the amide protons significantly. Therefore, gradient-enhanced NMR experiments that minimally perturbed the magnetization of water were absolutely essential for these studies (Grzesiek & Bax, 1993; Zhang et al., 1994). High ionic strength solution conditions of ~500 mM monovalent salt are required for the solubility of Ets-1 Δ N280. Based on the solution structure of Ets-1 Δ N331, there are distinct regions of negative and positive charges on the surfaces of these proteins that may result in the need for high salt concentrations to screen intermolecular electrostatic interactions (Donaldson et al., 1996).

¹H-¹H 2D NMR spectroscopy

2D NOESY (Macura et al., 1981) and clean-TOCSY (Griesinger et al., 1988) experiments were recorded on unlabeled Ets-1 Δ N280 in 99% ²H₂O. Low-power continuous radio-frequency irradiation with the carrier placed on the water resonance (4.70 ppm at 32 °C) was used to suppress the residual water signal. The NOESY spectrum was recorded with a 100-ms mixing time and the TOCSY was acquired with a 48 ms clean MLEV-17 mixing sequence. The ratio of clean-TOCSY delay to the mixing 90° pulse length was 1.5 with an average rf power for the spinlock of 8.8 kHz. Quadrature detection in t_1 was accomplished using the method of States et al. (1982).

Heteronuclear 2D ¹H-¹⁵N NMR spectroscopy

2D ¹H-¹⁵N HSQC spectra (Bodenhausen & Ruben, 1980) were acquired from uniformly ¹⁵N- or ¹³C/¹⁵N-labeled or selectively α -¹⁵N-Ala-, -Asn- and Asp-, -Leu-, -Lys-, -Tyr-, or

Table 2. Acquisition and processing parameters for NMR experiments recorded on Ets-1ΔN280^a

Experiments	Nucleus	Acq. pts.	Spec. width	Carrier freq.	Processing ^b	Matrix dim.
1H- ¹⁵ N-HSQC	$t_1 = ^{15}\text{N}$	128	1,250	121.42	ss(80°)	1,024
	$t_2 = ^1\text{H}^N$	1,024	6,250	4.70	tdc, gm, pol	1,024
1H- ¹⁵ N-HMQC-J	$t_1 = ^{15}\text{N}$	128	1,250	121.42	gm(-10, -15)	4,096
	$t_2 = ^1\text{H}^N$	1,024	6,250	4.70	tdc, gm(-5), pol	1,024
¹⁵ N-{ ¹ H}NOE	$t_1 = ^{15}\text{N}$	96	1,250	121.42	ss(80°)	1,024
	$t_2 = ^1\text{H}^N$	1,024	6,250	4.70	tdc, gm(-10), pol	1,024
¹⁵ N-NOESY-HSQC	$t_1 = ^{15}\text{N}$	96	6,250	4.70	lp, ss(80°)	512
	$t_2 = ^{15}\text{N}$	54	1,250	121.42	lp, ss(80°)	128
	$t_3 = ^1\text{H}^N$	512	6,250	4.70	tdc, gm(-7), pol	256
¹⁵ N-TOCSY-HSQC	$t_1 = ^1\text{H}$	96	6,250	4.70	lp, ss(80°)	512
	$t_2 = ^{15}\text{N}$	54	1,250	121.42	lp, ss(80°)	128
	$t_3 = ^1\text{H}^N$	512	6,250	4.70	tdc, gm(-7), pol	256
¹⁵ N/ ¹³ C-HNCO	$t_1 = ^{13}\text{C}'$	64	1,050	176.95	lp, ss(80°)	256
	$t_2 = ^{15}\text{N}$	ct 30	1,250	121.42	lp, ss(80°)	128
	$t_3 = ^1\text{H}^N$	512	6,250	4.70	tdc, gm(-5), pol	256
¹⁵ N/ ¹³ C-HNCACB	$t_1 = ^{13}\text{C}^{\alpha\beta}$	45	8,050	41.76	lp, ss(80°), em(6)	256
	$t_2 = ^{15}\text{N}$	ct 31	1,250	121.42	lp, ss(80°)	128
	$t_3 = ^1\text{H}^N$	512	6,250	4.70	tdc, gm(-5), pol	256
¹⁵ N/ ¹³ C-CBCA(CO)NH	$t_1 = ^{13}\text{C}^{\alpha\beta}$	53	8,050	41.76	lp, ss(80°), em(6)	256
	$t_2 = ^{15}\text{N}$	ct 31	1,250	121.42	lp, ss(80°)	128
	$t_3 = ^1\text{H}^N$	512	6,250	4.70	tdc, gm(-5), pol	256
¹ H/ ¹³ C-CBCACO(CA)HA	$t_1 = ^{13}\text{C}'$	40	1,050	176.95	lp, ss(80°), em(8)	256
	$t_2 = ^{13}\text{C}^{\alpha\beta}$	ct 54	8,050	41.76	lp, ss(80°), em(6)	256
	$t_3 = ^1\text{H}^\alpha$	512	6,250	4.70	gm(-5), pol	256
¹ H/ ¹³ C-HCCH-TOCSY	$t_1 = ^1\text{H}$	96	3,750	4.70	lp, ss(80°)	256
	$t_2 = ^{13}\text{C}$	41	4,025	41.76	lp, ss(80°), em(8)	256
	$t_3 = ^1\text{H}$	512	6,250	4.70	gm(-5), pol	512
¹ H- ¹ H-clean TOCSY	$t_1 = ^1\text{H}$	300	6,250	4.70	ss(80°)	1,024
	$t_2 = ^1\text{H}$	1,024	6,250	4.70	gm(-5), pol	1,024
¹ H- ¹ H-NOESY	$t_1 = ^1\text{H}$	250	6,250	4.70	ss(80°)	1,024
	$t_2 = ^1\text{H}$	1,024	6,250	4.70	gm(-5), pol	1,024

^a Parameters: acq. pts. (complex acquisition points); spectral width (Hz); carrier freq. (ppm); matrix dim. (final matrix size in real points).

^b Processing parameters: ct = constant time; lp = linear prediction (or mirror image linear prediction with constant time); ss = sinebell squared (degrees shifted); gm = Lorentzian-to-Gaussian multiplication with a maximum at 0.1 of the acquisition time (Hz line broadening); em = exponential multiplication (Hz line broadening); pol = polynomial baseline flattening; tdc = time domain convolution.

-Val-labeled Ets-1ΔN280 samples. Sensitivity-enhanced and pulsed-field gradient pulse sequences were employed (Muhandiram & Kay, 1994), along with selective “flip-back” pulses to return water magnetization to the +z-axis prior to acquisition of the NMR signal (Grzesiek & Bax, 1993). WALTZ16 modulation (Shaka et al., 1983) was used for ¹⁵N decoupling and hard pulses were used for ¹³C decoupling, when required. Quadrature detection in the indirect dimension was accomplished using the States-TPPI method (Marion et al., 1989). Steady-state ¹⁵N-{¹H}NOE values were obtained from sensitivity-enhanced 2D ¹H-¹⁵N correlation experiments, with minimal water perturbation (Kay et al., 1989; Farrow et al., 1994), recorded on uniformly ¹⁵N-labeled Ets-1ΔN280 at pH 6.4 and 28 °C. ¹H saturation was achieved using a 3 s train of 120° pulses spaced at 5 ms intervals, followed by data acquisition and a final 1 s recycle delay. A control spectrum was recorded without ¹H saturation using a 4 s recycle delay. The total acquisition time for each spectrum was 25 h. Peak volumes were integrated using FELIX 2.3 and the steady-state ¹⁵N-{¹H}NOE calculated as ($I_{\text{noe}}/I_{\text{control}}$).

¹⁵N-separated 3D NMR spectroscopy

3D ¹⁵N-separated TOCSY-HSQC and NOESY-HSQC (Fesik & Zuiderweg, 1990) were acquired on uniformly ¹⁵N-labeled samples of Ets-1ΔN280 in 90% H₂O/10% ²H₂O at pH 6.4 and 28 °C to optimize signal intensity. At pH 7.1 and 32 °C, the NOE crosspeaks were markedly weaker. The ¹H-¹⁵N chemical shifts in the ¹H-¹⁵N HSQC spectrum were nearly identical at pH 7.1, 32 °C and pH 6.4, 28 °C. The TOCSY-HSQC experiment was acquired using a 47 ms clean-DIPSI mixing sequence. The ratio of the clean-DIPSI delay and the DIPSI 90° pulse length was 1.6, with an average spinlock field strength of 9.2 kHz. The NOESY-HSQC was acquired using a 100 ms mixing time. Both experiments were recorded using sensitivity-enhanced and pulsed-field gradient versions designed for minimal perturbation of the water magnetization (Zhang et al., 1994).

Triple resonance NMR

3D HNCACB (Wittekind & Mueller, 1993), CBCA(CO)NH (Grzesiek & Bax, 1992), HNCO (Ikura et al., 1990; Muhandiram & Kay, 1994), CBCACO(CA)HA (Kay, 1993), and HCCH-

TOCSY (Bax et al., 1990; Kay et al., 1993) were acquired on a 0.7 mM uniformly $^{13}\text{C}/^{15}\text{N}$ -labeled Ets-1 $\Delta\text{N}280$ sample. For triple resonance experiments in which magnetization was detected on the amide H^{N} proton, pulsed-field gradient pulse sequences with sensitivity enhancement and minimal water perturbation were utilized (Grzesiek & Bax, 1993; Muhandiram & Kay, 1994). Initial timings in indirect dimensions were set to $1/(2 * \text{sw})$ exactly, resulting in first-order phase shifts of 180° and the inversion of aliased signals. Quadrature detection was accomplished in the indirect dimensions using the States-TPPI method (Marion et al., 1989). Each 3D triple resonance experiment was acquired for ~ 3 days.

Amide hydrogen exchange

Amide hydrogen exchange rates were measured by transferring uniformly ^{15}N -labeled Ets-1 $\Delta\text{N}280$ sample to $^2\text{H}_2\text{O}$ buffer ($\text{pH}^* 7.0$) using a Sephadex G-25 spin-column. Exchange of H_2O for $^2\text{H}_2\text{O}$ was approximately 95% based upon intensity of residual H_2O signal. A series of sensitivity-enhanced gradient $^1\text{H}-^{15}\text{N}$ HSQC spectra were acquired at 10, 170, 380, 700, and 2,300 min after exchange to $^2\text{H}_2\text{O}$.

Coupling constants

$^3J_{\text{HN-H}\alpha}$ coupling constants were measured from a $^1\text{H}-^{15}\text{N}$ HMQC-J spectrum (Kay & Bax, 1990). Data were processed in the ^{15}N dimension using a Lorentzian-to-Gaussian apodization function with -10 or -15 Hz line broadening and a maximum in the apodization function at 0.5 of the total ^{15}N acquisition time of 0.144 s. $^3J_{\text{HN-H}\alpha}$ were determined using software provided by Lewis Kay as described by Forman-Kay et al. (1990). Resolved signals that were not measurably split in the ^{15}N dimension were defined as $^3J_{\text{HN-H}\alpha} < 6$ Hz.

Note added in proof

The recent structural analysis of an Ets-1 ETS domain/DNA complex highlights the role of the N-terminus of helix H1 in DNA binding (Werner MH, Clore GM, Fisher CL, Fisher RJ, Trinh L, Shiloach J, Gronenborn AM. 1995. *Cell* 83:761-771).

Acknowledgments

We thank Lewis Kay for generously providing the NMR pulse sequences and software used in this study; Cyril Kay for performing the ultracentrifugation analysis; Linda Cuddeford for help with protein preparation; and Tom Alber, Peter Flynn, and Leigh Plesniak for helpful discussions and encouragement. This work was supported by grants from the National Cancer Institute of Canada with funds from the Canadian Cancer Society (L.P.M.) and the National Institutes of Health GM 38663 and CA 42014 (B.J.G. and University of Utah Cancer Center). Instrument support from the Protein Engineering Network of Centres of Excellence (L.P.M.) is gratefully acknowledged.

References

- Bai Y, Milne JS, Mayne L, Englander SW. 1993. Primary structure effects on peptide group hydrogen exchange. *Proteins Struct Funct Genet* 17: 75-86.
- Bax A, Clore GM, Gronenborn AM. 1990. $^1\text{H}-^1\text{H}$ correlation via isotropic mixing of ^{13}C magnetization, a new three-dimensional approach for assigning ^1H and ^{13}C spectra of ^{13}C -enriched proteins. *J Magn Reson* 88:425-431.
- Bodenhausen G, Ruben DJ. 1980. Natural abundance nitrogen-15 NMR by enhanced heteronuclear spectroscopy. *Chem Phys Lett* 69:185-189.
- Brennan RG. 1993. The winged-helix DNA-binding motif: Another helix-turn-helix takeoff. *Cell* 74:773-776.
- Clark KL, Halay ED, Lai E, Burley SK. 1993. Co-crystal structure of the HNF-3/forkhead DNA-recognition motif resembles histone H5. *Nature* 364:412-420.
- Dalton S, Treisman R. 1992. Characterization of SAP-1, a protein recruited by serum response factor to the c-fos serum response element. *Cell* 68: 597-612.
- Donaldson LW, Petersen JM, Graves BJ, McIntosh LP. 1994. Secondary structure of the ETS domain places murine Ets-1 in the superfamily of winged-helix-turn-helix DNA-binding proteins. *Biochemistry* 33:13509-13516.
- Donaldson LW, Petersen JM, Graves BJ, McIntosh LP. 1996. Solution structure of the ETS domain from murine Ets-1: A winged helix-turn-helix DNA binding motif. *EMBO J.* Forthcoming.
- Edelhoch H. 1967. Spectroscopic determination of tryptophan and tyrosine in proteins. *Biochemistry* 6:1948-1954.
- Farrow NA, Muhandiram DR, Singer AU, Pascal SM, Kay CM, Gish G, Shoelson SE, Pawson T, Foreman-Kay JD, Kay LE. 1994. Backbone dynamics of a free and phosphopeptide-complexed Src homology 2 domain studied by ^{15}N NMR relaxation. *Biochemistry* 33:5984-6003.
- Fesik SW, Zuiderweg ER. 1990. Heteronuclear three-dimensional NMR spectroscopy of isotopically labeled biological macromolecules. *Q Rev Biophys* 23:97-131.
- Fisher RJ, Fivash M, Casas-Finet J, Erickson JW, Kondoh A, Bladen SV, Fisher C, Watson DK, Papas TS. 1994. Real-time DNA binding measurements of the ETS1 recombinant oncoproteins reveal significant kinetic differences between the p42 and p51 isoforms. *Protein Sci* 3:257-266.
- Forman-Kay JD, Gronenborn AM, Kay LE, Wingfield PT, Clore GM. 1990. Studies on the solution conformation of human thioredoxin using heteronuclear $^{15}\text{N}-^1\text{H}$ nuclear magnetic resonance spectroscopy. *Biochemistry* 29:1566-1572.
- Giovane A, Pintzas A, Maira SM, Sobieszcuk P, Waslyk B. 1994. Net, a new ets transcription factor that is activated by Ras. *Genes & Dev* 8: 1502-1513.
- Griesinger G, Otting G, Wüthrich K, Ernst RR. 1988. Clean TOCSY for ^1H spin system identification in macromolecules. *J Am Chem Soc* 110:7870-7872.
- Grimm S, Baeuerle PA. 1993. The inducible transcription factor NF-kappa B: Structure-function relationship of its protein subunits. *Biochem J* 290:297-308.
- Grzesiek S, Bax A. 1992. Correlating backbone amide and side chain resonances in larger proteins by multiple relayed triple resonance NMR. *J Am Chem Soc* 114:6291-6293.
- Grzesiek S, Bax A. 1993. The importance of not saturating H_2O in protein NMR. Application to sensitivity enhancement and NOE measurements. *J Am Chem Soc* 115:12593-12594.
- Hagman J, Grosschedl R. 1992. An inhibitory carboxy-terminal domain in Ets-1 and Ets-2 mediates differential binding of ETS family factors to promoter sequences of the *mb-1* gene. *Proc Natl Acad Sci USA* 89:8889-8893.
- Hahn SL, Waslyk B. 1994. The oncoprotein v-Ets is less selective in DNA binding than c-Ets-1 due to the C-terminal sequence change. *Oncogene* 9: 2499-2512.
- Hupp TR, Meek DW, Midgley CA, Lane CP. 1992. Regulation of the specific DNA binding function of p53. *Cell* 71:875-886.
- Ikura M, Kay LE, Bax A. 1990. A novel approach for sequential assignment of ^1H , ^{13}C , and ^{15}N spectra of proteins: Heteronuclear triple-resonance three-dimensional NMR spectroscopy. Application to calmodulin. *Biochemistry* 29:4659-4667.
- Janknecht R, Nordheim A. 1993. Gene regulation by Ets proteins. *Biochim Biophys Acta* 1155:346-356.
- Janknecht R, Zinck R, Ernst WH, Nordheim A. 1994. Functional dissection of the transcription factor Elk-1. *Oncogene* 9:1273-1278.
- Jonsen MD, Petersen JM, Xu Q-P, Graves BJ. 1996. Characterization of the cooperative function of inhibitory sequences in Ets-1. Submitted.
- Jorcyk CL, Watson DK, Mavrothalassitis GJ, Papas TS. 1991. The human ETS1 gene: Genomic structure, promoter characterization and alternative splicing. *Oncogene* 6:523-532.
- Karim FD, Urness LD, Thummel CS, Klemsz MJ, McKercher SR, Celada A, Beveren CV, Maki RA, Gunther CV, Nye JA, Graves BJ. 1990. The ETS-domain: A new DNA-binding motif that recognizes a purine-rich core DNA sequence. *Genes & Dev* 4:1451-1453.
- Kay LE. 1993. Pulsed-field gradient-enhanced three-dimensional NMR experiment for correlating $^{13}\text{C}\alpha/\beta$, ^{13}C , and $^1\text{H}\alpha$ chemical shifts in uniformly ^{13}C labeled proteins dissolved in H_2O . *J Am Chem Soc* 115: 2055-2057.
- Kay LE, Bax A. 1990. New methods for the measuring of NH-C α H coupling constants in ^{15}N -labeled proteins. *J Magn Reson* 86:110-126.

- Kay LE, Torchia DA, Bax A. 1989. Backbone dynamics of proteins as studied by ^{15}N inverse detected heteronuclear NMR spectroscopy: Application to staphylococcal nuclease. *Biochemistry* 28:8972–8979.
- Kay LE, Xu GY, Singer AU, Muhandiram DR, Forman-Kay JD. 1993. A gradient-enhanced HCCH-TOCSY experiment for recording side-chains ^1H and ^{13}C correlations in H_2O samples of proteins. *J Magn Reson* 101:333–337.
- Kowenz-Leutz E, Twamley G, Ansieau S, Leutz A. 1994. Novel mechanism of C/EBP (NF-M) transcriptional control: Activation through derepression. *Genes & Dev* 8:2781–2791.
- Leprince D, Crepieux P, Lauden V, Flourens A, Stehelin D. 1993. A new mechanism of oncogenic activation: E26 retroviral v-ets oncogene has inverted the C-terminal end of the transcription factor c-ets-1. *Virology* 194: 855–857.
- Leprince D, Crepieux P, Stehelin D. 1992. C-ets-1 DNA binding to the PEA3 motif is differentially inhibited by all the mutations found in v-ets. *Oncogene* 7:9–17.
- Leprince D, Gegonne A, Coll J, Scheeberger A, Lagrou C, Stehelin D. 1983. A putative second cell-derived oncogene of the avian leukemia retrovirus E26. *Nature* 306:395–397.
- Liang H, Mao X, Olejniczak ET, Nettesheim DG, Yu L, Meadows RP, Thompson CB, Fesik SW. 1994a. Solution structure of the Ets domain of Fli-1 when bound to DNA. *Nature Struct Biol* 1:871–875.
- Liang H, Olejniczak ET, Mao X, Nettesheim DG, Yu L, Thompson CB, Fesik SW. 1994b. The secondary structure of the ets domain of human Fli-1 resembles that of the helix-turn-helix DNA-binding motif of the *Escherichia coli* catabolite gene activator protein. *Proc Natl Acad Sci USA* 91:11655–11659.
- Lieberman PM, Schmidt MC, Kao CC, Berk AJ. 1991. Two distinct domains in the yeast transcription factor IID and evidence for a TATA box-induced conformational change. *Mol Cell Biol* 11:63–74.
- Lim F, Kraut N, Frampton J, Graf T. 1992. DNA binding by c-Ets-1, but not v-Ets, is repressed by an intramolecular mechanism. *EMBO J* 11: 643–652.
- Lopez M, Oettgen P, Akbarali Y, Dendorfer U, Libermann TA. 1994. ERP, a new member of the est transcription factor/oncoprotein family: Cloning, characterization, and differential expression during B-lymphocyte development. *Mol Cell Biol* 14:3292–3309.
- Macleod K, Leprince D, Stehelin D. 1992. The ets gene family. *Trends Biochem Sci* 17:251–256.
- Macura S, Huang Y, Suter D, Ernst RR. 1981. Two-dimensional chemical exchange and cross-relaxation spectroscopy of coupled nuclear spins. *J Magn Reson* 43:259–281.
- Marion D, Ikura M, Tschudin R, Bax A. 1989. Rapid recording of 2D NMR spectra without phase cycling. Application to the study of hydrogen exchange in proteins. *J Magn Reson* 85:393–399.
- McIntosh LP, Dahlquist FW. 1990. Biosynthetic incorporation of ^{15}N and ^{13}C for assignment and interpretation of nuclear magnetic resonance spectra of proteins. *Q Rev Biophys* 23:1–38.
- McIntosh LP, Wand AJ, Lowry DF, Redfield AG, Dahlquist FW. 1990. Assignment of the backbone ^1H and ^{15}N NMR resonances of bacteriophage T4 lysozyme. *Biochemistry* 29:6341–6362.
- Muhandiram DR, Kay LE. 1994. Gradient-enhanced triple-resonance three-dimensional NMR experiments with improved sensitivity. *J Magn Reson Ser B* 103:203–216.
- Nicholls A, Sharp KA, Honig B. 1991. Protein folding and association: Insights from the interfacial and thermodynamic properties of hydrocarbons. *Proteins Struct Funct Genet* 11:281–296.
- Nunn MF, Hunter T. 1989. The ets sequence is required for induction of erythroblastosis in chickens by avian retrovirus E26. *J Virol* 63:398–402.
- Nunn MF, Seeburg PH, Moscovici C, Duesberg PH. 1983. Tripartite structure of the avian erythroblastosis virus E26 transforming gene. *Nature* 306:391–397.
- Nye JA, Petersen JM, Gunther CV, Jonsen MD, Graves BJ. 1992. Interaction of murine Ets-1 with GGA-binding sites establishes the ETS domain as a new DNA-binding motif. *Genes & Dev* 6:975–990.
- Olejniczak ET, Fesik SW. 1994. Two-dimensional nuclear magnetic resonance method for identifying the $\text{H}\alpha/\text{C}\alpha$ signals of amino acid residues preceding proline. *J Am Chem Soc* 116:2215–2216.
- Petersen JM, Skalicky JJ, Donaldson LW, McIntosh LP, Alber T, Graves BJ. 1995. Modulation of transcription factor Ets-1 DNA binding: DNA-induced unfolding of an α helix. *Science* 269:1866–1869.
- Rabindran SK, Haroun RI, Clos J, Wisniewski J, Wu C. 1993. Regulation of heat shock factor trimer formation: Role of a conserved leucine zipper. *Science* 259:230–234.
- Richardson JS. 1981. The anatomy and taxonomy of protein structure. *Adv Protein Chem* 34:167–339.
- Schultz SC, Shields GC, Steitz TA. 1991. Crystal structure of a CAP-DNA complex: The DNA is bent by 90°. *Science* 253:1001–1007.
- Shaka AJ, Keeler J, Freeman R. 1983. Evaluation of a new broadband decoupling sequence: Waltz16. *J Magn Reson* 53:313–340.
- States DJ, Haberkorn RA, Ruben DJ. 1982. A two-dimensional nuclear Overhauser experiment with pure absorption phase in four quadrants. *J Magn Reson* 48:286–292.
- Wasyluk B, Hahn S, Giovane A. 1993. The Ets family of transcription factors. *Eur J Biochem* 211:7–18.
- Wasyluk C, Kerckaert JP, Wasyluk B. 1992. A novel modulator domain of Ets transcription factors. *Genes & Dev* 6:965–974.
- Watson DK, McWilliams MJ, Lapis P, Lautenberger JA, Scheinfest CW, Papas TS. 1988. Mammalian ets-1 and ets-2 genes encode highly conserved proteins. *Proc Natl Acad Sci USA* 85:7862–7866.
- Williams SC, Baer M, Dillner AJ, Johnson PF. 1995. CRP(C/EBP β) contains a bipartite regulatory domain that controls transcriptional activation, DNA binding and cell specificity. *EMBO J* 14:3170–3183.
- Wishart DS, Sykes BD. 1994. The ^{13}C chemical-shift index: A simple method for the identification of protein secondary structure using ^{13}C chemical-shift data. *J Biomol NMR* 4:171–180.
- Wishart DS, Sykes BD, Richards FM. 1992. The chemical shift index: A fast and simple method for the assignment of protein secondary structure through NMR spectroscopy. *Biochemistry* 31:1647–1651.
- Wittekind MG, Mueller L. 1993. HNCACB, a high-sensitivity 3D NMR experiment to correlate amide-proton and nitrogen resonances with the alpha- and beta-carbon resonances. *J Magn Reson Ser B* 101:201–205.
- Wüthrich K. 1986. *NMR of proteins and nucleic acids*. New York: J. Wiley & Sons.
- Zhang O, Kay LE, Olivier JP, Forman-Kay JD. 1994. Backbone ^1H and ^{15}N resonance assignments of the N-terminal SH3 domains of drk in folded and unfolded states using enhanced-sensitivity pulsed field gradient NMR techniques. *J Biomol NMR* 4:845–858.